IMPROVING FLUID REGISTRATION THROUGH WHITE MATTER SEGMENTATION

Yi-Yu Chou[1], *Natasha Leporé*[1], *Caroline C. Brun*[1], *Agatha D. Lee*[1], *Marina Barysheva*[1], *Greig I. de Zubicaray*[2], *Katie McMahon*[2], *Margaret J. Wright*[3], *Arthur W. Toga*[1], *Paul M. Thompson*[1]

[1]Laboratory of Neuro Imaging, UCLA Dept. of Neurology, Los Angeles, CA, USA
[2]Centre for Magnetic Resonance, University of Queensland, Brisbane, Australia
[3]Genetic Epidemiology Laboratory, Queensland Institute of Medical Research, Brisbane, Australia

ABSTRACT

Robust and automatic non-rigid registration depends on many parameters that have not yet been systematically explored. Here we determined how tissue classification influences non-linear fluid registration of brain MRI. Twin data is ideal for studying this question, as volumetric correlations between corresponding brain regions that are under genetic control should be higher in monozygotic twins (MZ) who share 100% of their genes when compared to dizygotic twins (DZ) who share half their genes on average. When these substructure volumes are quantified using tensor-based morphometry, improved registration can be defined based on which method gives higher MZ twin correlations when compared to DZs, as registration errors tend to deplete these correlations. In a study of 92 subjects, higher effect sizes were found in cumulative distribution functions derived from statistical maps when performing tissue classification before fluid registration, versus fluidly registering the raw images. This gives empirical evidence in favor of pre-segmenting images for tensor-based morphometry.

Index Terms— tissue classification, registration, MRI, twin study

1. INTRODUCTION

Tensor-based morphometry (TBM) is now widely used in morphometric studies, providing detailed maps of volumetric differences between groups of subjects scanned with structural MRI in diseases such as Alzheimer's disease, HIV/AIDS, and mapping abnormal brain changes over time in childhood development [1].

Many studies have attempted to optimize statistical power for detecting disease effects in TBM, as many of the effect sizes of interest are very small. For instance, a recent TBM study of 676 subjects found that the ApoE2 gene is protective against brain atrophy in Alzheimer's disease, and other large TBM studies have associated subtle alterations in brain structure to clinical outcomes, medication effects, and even immune system measures [2].

Many attempts to boost effect sizes in TBM have focused on computing multivariate statistics from the deformation tensor [3], or improving the deformation models to include different regularization schemes such as Riemannian fluid models [4], improving the template to which all images are aligned [5] or improving the pre- processing of MRI data to maximize longitudinal stability [6].

Even so, one unanswered empirical question in TBM is whether the MR images should be pre-segmented into gray and white matter and CSF, or whether greater power is gained by running fluid registration on the raw images. Tissue classification has been used in many registration approaches [7], largely motivated by computational efficiency, as it avoids computing gradients of the cost function in homogeneous regions.

Here we performed an analysis to quantify whether it helps to use a tissue classification as an initial step in the registration. We performed tensor based morphometry in a twin study design, where registration errors tend to deplete the effect sizes for intra-pair correlations. As genetic factors cause twins who share half or all of their genes to resemble each other in brain structure [4], there is great interest in finding the relevant genes after first identifying heritable aspects of brain structure. Both of these efforts require large samples and processing pipelines optimized for statistical power.

2. MATERIALS & METHODS

2.1 Overview

T1-weighted volumetric MRIs of 23 MZ and 23 DZ same-sex twin pairs were aligned to the Colin27 single-subject average brain template [8] by 9-parameter linear transformation. After preprocessing, the white matter (WM) was segmented using the modified mixture model cluster analysis technique in SPM5 [9]. Each individual's (1) whole brain volume and (2) binarized WM volume was non-linearly warped to a common randomly picked subject's whole brain or binary WM volume using a 3D Riemannian fluid registration algorithm [4]. For both segmented and non-segmented data, we created statistical maps from the

determinants of the deformation fields using the intraclass correlation (ICC) computed independently for the MZ and DZ groups.

2.2. Subjects

3D structural brain MRI scans were acquired from 23 MZ and 23 DZ same-sex twin pairs (age: 22-25 years) who received clinical evaluations and high-resolution MR scans as part of a 5-year research study of 700 pairs of twins. At the time of testing the twins were between the ages of 21 and 27 years (mean age: 23.8 years). Zygosity was established objectively by typing nine independent DNA microsatellite polymorphisms (PIC > 0.7) by using standard polymerase chain reaction (PCR) methods and genotyping. These results were crossed checked with blood group (ABO, MNS and Rh), and phenotypic data (hair, skin and eye color), giving an overall probability of correct zygosity assignment of greater than 99.99%. MR images were collected using a 4 Tesla Bruker Medspec whole body scanner (Bruker Medical, Ettingen, Germany) at the Center for Magnetic Resonance (University of Queensland, Australia). Three-dimensional T1-weighted images were acquired with an inversion recovery rapid gradient echo; MP-RAGE) to resolve anatomy at high resolution. Acquisition parameters were as follows: inversion time (T1)/repetition time (TR)/echo time (TE) = 1500/2500/3.83 msec; flip angle=15 degrees; slice thickness = 0.9mm with a 256 x 256 x 256 acquisition matrix.

Extracerebral tissues were manually deleted from the MRI scans using Display (Montreal Neurological Institute, McGill University, Canada). All scans were then aligned to the Colin27 average brain template using 9-parameter registration (i.e., translational and rotational alignment, allowing scaling in 3 independent directions) found in the FMRIB's Linear Image Registration Toolbox, FLIRT [10].

2.3. Segmentation

White matter segmentation was performed using the SPM5 software (Wellcome Department of Cognitive Neurology, London, UK, http://www.fil.ion.ucl.ac.uk/spm). SPM proceeds with an iterative probabilistic estimation of each voxel's classification using a Bayesian Gaussian mixture model, based on a prior probability image generated by averaging the image intensities for large number of subjects [9,11]. The resulting probability is interpreted as the probability of each voxel belonging to one of three tissue types – GM/WM/CSF. Here we set the probability > 0.5 to create a binary mask representing white matter regions.

2.4. Riemannian Fluid Registration

We followed the approach proposed in [4] to deform each of the images to a common space, using a single subject's scan as a target image. We preferred a single subject target to a population mean image to ensure similar contrast and features between the target and the individual images. In [4], we introduced a Riemannian fluid model in a multivariate Log-Euclidean framework. The deformation velocity $\vec{v}(x,')$ is computed and integrated in time to obtain the displacement $\vec{u}$ at position $\vec{x}$ using:

$$\frac{d\vec{v}(\vec{x},t)}{dt} = F(\vec{x},\vec{u}) + \nabla \mathrm{Re}\, g(\vec{v},t) - \vec{v}(x,')$$

where

$$\nabla \mathrm{Re}\, g(\vec{v},t) = \int \frac{\mu}{4} Tr(\log((\nabla\vec{v}+Id)^T(\nabla\vec{v}+Id))^2 + \frac{\lambda}{8} Tr(\log((\nabla\vec{v}+Id)^T(\nabla\vec{v}+Id)))^2 .$$

Here $F(\vec{x},\vec{u})$ denotes the force field that varies with the position $\vec{x}$ and drives the deformation $\vec{u}$, and *Reg* the log-Euclidean Riemannian regularizer, and μ and λ are viscosity constants.

The body force that drives the registration is defined as the gradient of the summed squared differences in intensities between the deforming template T(x-u(x,t)) and target S(x):

$$F((x,u(x,t)) = -(T(x-u(x,t)) - S(x))\nabla T\,|_{x-u(x,t)}$$

2.4. Statistical Analysis

The Jacobian determinants derived from the deformation fields were computed at each voxel to assess local volumetric differences between individuals with respect to the reference image. To measure the resemblance between twin pairs with different degrees of genetic similarity, we computed the intraclass correlation coefficient (ICC) for both the MZ and DZ groups. The ICC is defined as:

$$\rho = \frac{\sigma_b^2}{\sigma_b^2 + \sigma_w^2}$$

Here σ_b^2 is the pooled variance between pairs and σ_w^2 is the variance of the traits within pairs, which is the mean-

square estimate of within-pair variance. $\sigma_b^2 + \sigma_w^2$ is the total variance of the measures.

Statistical maps were generated indicating the p-values at each voxel describing the significance of the ICC values by randomly reassigning subject labels (5000 permutations) and computing nonparametric *p*-values from this null reference distribution. Cumulative Distribution Function (CDF) plots of the *p*-values were generated in order to assess statistical power. The value at which the CDF intersects the $y = 20x$ line represents the highest statistical threshold for which at most 5% false positives are expected in the map (controlling the false discovery rate) [12].

3. RESULTS

The *p*-values in **Figure 1** indicate the statistical significance of the correlations (voxels with $p < 0.05$ are shown in red) for the whole brain- (*top panel*) and WM- (*bottom panel*) based registrations. As expected, the *p*-values are generally lower in the MZ twins (denoting higher intraclass correlations) who share 100% of their genes. **Figure 2** shows the CDF plots of the *p*-values for ICC(MZ). For a null distribution, the cumulative distribution function is expected to fall approximately along the $x = y$ line. The larger upward deviations from the diagonal observed for the WM-based registration indicate greater statistical power and larger effect sizes (**Figure 2**).

In addition, permutation-based *p*-values were computed by scrambling the pairings and randomly reassigning a twin to each subject, i.e. by generating a nonparametric null distribution at each voxel to confirm the null CDF. Both the whole brain- and WM-based registrations give no change when no change is present (**Figure 2**). This test is useful because a method with greater effect sizes is only more useful if it can be shown to control the false positive rate correctly when no group difference is present.

4. DISCUSSION

Setting the whole WM class to the same value in MRI registration is sensible, since MR intensity differences are generally not reliable inside the WM, unless specialized sequences such as relaxometry or diffusion tensor imaging are used that are sensitive to white matter microstructure. When the WM is binarized, the effect of RF shading artifacts can be accommodated in the tissue classification, and the registration cost function has a stable gradient with a sharp global minimum. As noted by others [7], convergence is faster and CPU time is reduced, as the cost function can be set to zero in overlapping binary regions. This empirical data supports pre-classification of data when registration is used.

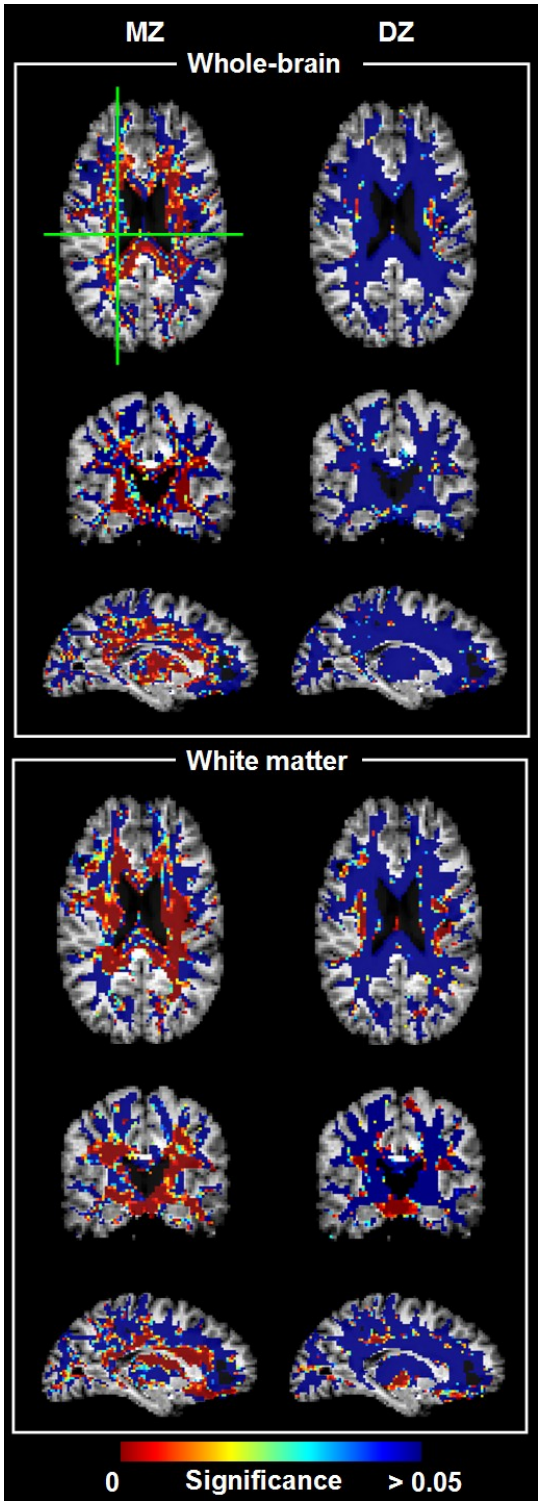

Fig. 1. Significance maps in 3 orthogonal sections for the intra-pair correlations in regional brain volumes, for MZ (*left column*) and DZ (*right column*) twin pairs after using registrations based on the whole brain (*top panel*; only the white matter p-values are shown) and WM (*bottom panel*).

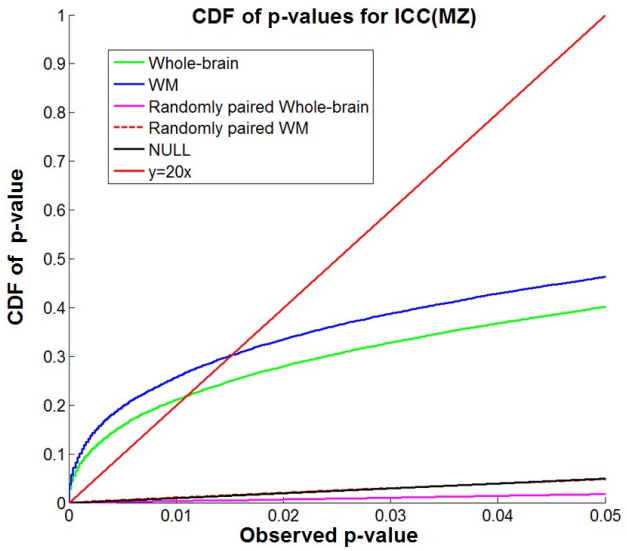

Fig.2. Cumulative Distribution Functions (CDFs) of significance maps for the ICC(MZ) and the null distribution of statistics when the twin subjects are randomly paired (i.e., when no correlation is truly present; red dash curve overlaps with the black line). Effect sizes are greater when the images are pre-segmented to produce binary tissue classifications. The two null lines show that both methods correctly control the false positive rate, when by construction, no correlations are present.

5. REFERENCES

[1] Gogtay N*, Lu A*, Leow AD, Klunder AD, Lee AD, Chavez A, Greenstein D, Giedd JN, Toga AW, Rapoport JL, Thompson PM (2008). *3D Growth Pattern Abnormalities Visualized in Childhood-Onset Schizophrenia using Tensor-Based Morphometry*, **Proceedings of the National Academy of Sciences,** published online, August 28 2008. [*equal contribution]

[2] Hua X, Leow AD, Parikshak N, Lee S, Chiang MC, Toga AW, Jack CR, Weiner MW, Thompson PM (2008). *Tensor-Based Morphometry as a Neuroimaging Biomarker for Alzheimer's Disease: An MRI Study of 676 AD, MCI, and Normal Subjects,* **NeuroImage**, 2008 Jul 22. [Epub ahead of print].

[3] Lepore N, Brun CC, Chou YY, Chiang MC, Dutton RA, Hayashi KM, Lu A, Lopez OL, Aizenstein HJ, Toga AW, Becker JT, Thompson PM (2008). *Generalized Tensor-Based Morphometry of HIV/AIDS Using Multivariate Statistics on Deformation Tensors*, **IEEE Transactions on Medical Imaging**, 27(1):129-141.

[4] Brun C et al. (2007). Comparison of Standard and Riemannian elasticity for Tensor-Based Morphometry in HIV/AIDS, MICCAI workshop on Statistical Registration: Pair-wise and Group-wise Alignment and Atlas Formation.

[5] Lepore N, Brun CC, Pennec X, Chou YY, Lopez OL, Aizenstein HJ, Becker JT, Toga AW, Thompson PM (2007). *Mean Template for Tensor-Based Morphometry using Deformation Tensors*, **MICCAI 2007**.

[6] Leow AD, Klunder AD, Jack CR, Toga AW, Dale AM, Bernstein MA, Britson PJ, Gunter JL, Ward CP, Whitwell JL, Borowski B, Fleisher A, Fox NC, Harvey D, Kornak J, Schuff N, Studholme C, Alexander GE, Weiner MW, Thompson PM (2006). *Longitudinal Stability of MRI for Mapping Brain Change using Tensor-Based Morphometry*, **NeuroImage**, 2006 Feb 7.

[7] Kochunov P, Lancaster J, Thompson PM, Boyer A, Hardies J, Fox PT (2000). *Validation of an Octree Regional Spatial Normalization Method for Regional Anatomical Matching,* **Human Brain Mapping 11(3):**193-206.

[8] Holmes CJ, Hoge R, Collins L, Woods R, Toga AW, (1998). Evans AC. Enhancement of MR images using registration for signal averaging. JCAT 22(2):324-33.

[9] Ashburner J, Friston KJ (1997). *Multimodal Image Coregistration and Partitioning - a Unified Framework*. **NeuroImage** 6(3):209–217.

[10] Jenkinson, M et al. (2002). *Improved Optimization for the Robust and Accurate Linear Registration and Motion Correction of Brain Images.* **NeuroImage** 17(2), 825-841.

[11] Ashburner J, Friston KJ., (2000). *Voxel-Based Morphometry -- The Methods.* **NeuroImage** (11):805-821.

[12] Benjamini, Y., Hochberg, Y., (1995), *Controlling the False Discovery Rate: A Practical and Powerful Approach to Multiple Testing*. **J. Royal Stat Soc Series B**, 57:289-300.